TIME DOMAIN ANALYSIS OF PLASMA TURBULENCE OBSERVED UPSTREAM OF A QUASI-PARALLEL SHOCK

D. COCA M. BALIKHIN S.A. BILLINGS H.StC. ALLEYNE
Department of Automatic Control and Systems Engineering,
University of Sheffield
Sheffield, S1 3JD,
UK

M. DUNLOP
Imperial College London, SW7 2BZ, UK

Research Report No. 783
October 2000

Time Domain Analysis of Plasma Turbulence Observed Upstream of a Quasi-Parallel Shock

D. COCA[1] M. BALIKHIN S.A. BILLINGS H.StC. ALLEYNE
Department of Automatic Control and Systems Engineering,
University of Sheffield,
Sheffield S1 3JD, UK

M. DUNLOP
Imperial College London, SW7 2BZ, UK

Abstract

This paper presents, for the first time, an analysis of space plasma turbulence based on the NARMAX system identification approach. Fundamental nonlinear processes in the low frequency turbulence observed in the terrestrial fore-shock by AMPTE UKS and AMPTE IRM satellites are studied using time-domain identification methods developed for nonlinear dynamical systems. It is shown, directly from the experimental data, that the cubic nonlinearity has a significant influence on the steepening of the nonlinear low frequency waves and on the dependence of the phase velocity upon the wave amplitude. In comparison with a previous frequency domain approach the present method requires only short data sets.

1 Introduction

The ultimate goal of the experimental investigation of space plasma turbulence is to provide a complete quantitative description of the composition of turbulence (distribution of energy between various plasma modes) and the processes of energy transfer in it. The latter can be subdivided into two fundamental groups. The first group of processes includes energy exchange between turbulence and plasma particles due to plasma instabilities. Such processes can be considered as linear in the analysis of the plasma turbulence since this does not require multi-wave coupling or energy exchange between various scales of turbulence. The strength of such processes is characterized by linear growth (damping) rates. The second group includes nonlinear processes of the wave-wave interaction which provide energy transfer between various modes and scales. Three wave coupling (e.g. decay instability) corresponds to a quadratic nonlinearity. Four wave interactions (e.g. modulational instability) corresponds to a cubic nonlinearity. In the case of weak turbulence the consideration of nonlinear processes can be safely limited only to the processes which involve not more than four waves. Processes which involve five or more waves can be disregarded for such turbulence because the time scale associated with the action of a particular process increases with the number of waves involved. [*Zakharov, et al.*,1985].

All previous estimations of these parameters from multi-point measurements were based on direct frequency domain modelling approaches. For example [*McCaffrey et al.*, 1999] for dispersive turbulence and [*Dudok de Wit et al.*, 1999] (DW) for non-dispersive turbulence. The main disadvantage of these methods is that modelling in the frequency domain involves solutions of ill posed problems and requires very long series of stationary

[1]e-mail:coca@acse.shef.ac.uk

data to provide reliable results. Such a strict requirement resulted in the absence in the literature of even a single example in which the application of this method leads to the estimation of the strength of three and four wave processes in space plasma. Only in the case in which four wave processes can be disregarded can reliable results be obtained on data sets of a realistic length [*McCaffrey et al.,* 1999]. However when the role of the four wave processes is significant even the combination of all three components of the magnetic field data in one surrogate data set for such a huge region as an ion fore-shock failed to provide a data set long enough to estimate the strength of the four wave processes (DW).

In this paper we propose a new approach in the study of plasma turbulence using a well established time-domain nonlinear system identification method based on the NARMAX model [*Leontaritis and Billings,* 1987]. This method provides reliable results even for short data series. We applied this method to the developed turbulence observed in the terrestrial fore-shock populated by diffusive ions. This region of application was chosen for three reasons. First because it is saturated by the fundamental plasma turbulence processes. Instability caused by the ion distribution leads to energy exchange between plasma waves and ions. Manifestations of nonlinear wave coupling such as steepening of waves and the generation of wave trains in schocklets [*Hope and Russell,* 1983] ensures significant energy transfer between various modes (and or scales) of turbulence. In particular, high order spectral analysis results indicate that three wave processes can not be disregarded. The second reason was that in spite of the complexity of the turbulent dynamics and absence of complete experimental data very comprehensive theories of the processes in that region exist. The comparison between our results obtained from experimental data with existing theoretical models of the processes involved can be considered as an extra validation tool for our approach, reinforcing the standard model validation methods in nonlinear system identification. The third reason is that it allows a comprehensive comparison of our results with the results obtained via the direct multi-spectrum frequency domain modelling approach recently applied to the same interval of data (DW).

2 Brief description of the method and the data

The data used in this study were obtained by the AMPTE (Active Magnetospheric Particle Tracer Explorer) satellites UKS (United Kingdom Sub-satellite) and IRM (Ion Release Module). The data sets came from the magnetometer instruments on board each spacecraft. The UKS fluxgate magnetometer [*Southwood et al.,* 1985] was a modified version of the ISEE 1/2 instrument. The IRM fluxgate magnetometer was described in *Lühr et al.,* [1985]. The data used in the present study were gathered on day 304 of 1984 (October 30) upstream of the quasi-parallel part of the terrestrial bow shock. This particular event was intensively studied in several publications [*Schwartz and Burgess* 1991; *Schwartz et al.,* 1992; *Mann et al.,* 1994; *Dudok de Wit et al.,* 1995, 1999]. In particular DW was devoted to the identification of nonlinear processes in the fore-shock turbulence using modelling in frequency space. The magnitude and three components of the magnetic field as measured by AMPTE UKS and AMPTE IRM are plotted in Figure 1. The uniqueness of these data explains why so many studies have already been devoted to that particular event. The solar wind speed and magnetic field remained stable [*Schwartz et al.,* 1992]. The spacecraft separation vector was nearly parallel with the GSE x-axis. During the whole period under investigation the orientation of averaged IMF remained in the quasi-parallel regime and the angle between the magnetic field and the model shock normal was 10°-

15° [*it Schwartz et al.,* 1992]. The stability of these conditions enables the application of a "black box" nonlinear system identification approach, which in this particular case can be formulated as follows. After being detected by the first satellite (AMPTE UKS) waves propagate in the plasma, where they are affected by the plasma instabilities and the energy transfer processes within the turbulence itself. The accumulated effect of all these processes is measured by the second satellite (AMPTE IRM). In this context the measurements of AMPTE UKS and AMPTE IRM can be considered as input and output of a black box system. The spectral components measured by the satellites should be related by the following equation [*Ritz and Powers,* 1986]:

$$B_{\omega}^{irm} = L_{\omega} B_{uks}^{\omega} + \sum_{\substack{\omega_1,\omega_2 \\ \omega_1+\omega_2=\omega}} Q_{\omega}^{\omega_1,\omega_2} B_{uks}^{\omega_1} B_{uks}^{\omega_2} + \sum_{\substack{\omega_1,\omega_2,\omega_3 \\ \omega_1+\omega_2+\omega_3=\omega}} T_{\omega}^{\omega_1,\omega_2,\omega_3} B_{uks}^{\omega_1} B_{uks}^{\omega_2} B_{uks}^{\omega_3} \quad (1)$$

The first term on the right hand (r.h.s.) describes linear effects such as propagation and growth (damping). The second term on the r.h.s. is due to the quadratic nonlinearity and corresponds to the three wave coupling of the decay instability type in which two waves at frequencies ω_1 and ω_2 transfer their energy to the wave on a summation frequency. Similarly, the third term is a result of four wave interactions or cubic nonlinearity, which involves interaction of three waves with energy transfer to the fourth one. The spectral domain method proposed by *Ritz and Powers* [1986], which was used in DW, was based on the solution of the system of linear equations similar to (1), in which L_{ω}, $Q_{\omega}^{\omega_1,\omega_2}$ and $T_{\omega}^{\omega_1,\omega_2,\omega_3}$ are unknown variables. Amplitudes of spectral components $B_{uks}^{\omega_i}$ and $B_{irm}^{\omega_i}$ can be estimated directly from measurements. As mentioned above the resulting system of equations is ill posed and the standard regularisation procedure requires a very long data series. The alternative approach, which we used in the present paper, is based on the estimation of a time domain relation between discrete measurements of AMPTE-UKS B_{uks} and AMPTE-IRM B_{irm}. This time-domain model can subsequently be mapped into the frequency domain using the *Volterra series representation* which allows L_{ω}, $Q_{\omega}^{\omega_1,\omega_2}$ and $T_{\omega}^{\omega_1,\omega_2,\omega_3}$ to be calculated analytically.

A linear dynamical system can be described as a convolution of the input $u(t)$ and the impulse response function $h(t)$

$$y(t) = \int_0^{\infty} h(\tau) u(t-\tau) d\tau \quad (2)$$

In the case of discrete measurements this will take the form

$$y(k) = \sum_{i=1}^{\infty} h(i) u(k-i) \quad (3)$$

where $h(k)$ is the discrete impulse response. The Fourier transform $H(j\omega)$ of $h(\tau)$ which relates the spectral components of the input and the output $y(j\omega) = H(j\omega)u(j\omega)$ is the linear frequency response function ($H(j\omega) = H_{lin}(j\omega) = L(\omega)$). An alternative and more concise representation of (3) which does not involve infinite series is the linear difference equation model

$$y(k) = \sum_{i=1}^{n_y} a_i y(k-i) + \sum_{i=1}^{n_u} b_i u(k-i) \quad (4)$$

The coefficients of the model in equation (4) can be estimated from a set of input and output measurements using least-squares type algorithms. A generalisation of the convo-

lution integral in equation (2) to nonlinear dynamical systems is the Volterra series

$$y(t) = \int_0^\infty h_1(\tau)u(t-\tau)d\tau + \int_0^\infty \int_0^\infty h_2(\tau_1,\tau_2)u(t-\tau_1)u(t-\tau_2)d\tau_1 d\tau_2 + ... \quad (5)$$

The Fourier transforms of the Volterra kernels $H_1(j\omega)$, $H_2(j\omega_1, j\omega_2)$,...,$H_n(j\omega_1, ..., j\omega_n)$... define the Generalised Frequency Response Functions of the nonlinear system. While $H_1(j\omega)$ has the same meaning as $H_{lin}(j\omega)$ for a linear system, the higher order frequency response functions describe the energy transfer between tuples of input frequencies $\omega_1, ..., \omega_n$ to the output frequency $\omega = \sum_{i=1}^n \omega_i$. Therefore $H_2(j\omega_1, j\omega_2)$ is equivalent to $Q_\omega^{\omega_1,\omega_2}$ and H_3 is equivalent to $T_\omega^{\omega_1,\omega_2,\omega_3}$ in equation (1).

A finite dimensional input-output realisation of (5) is often much more suitable for practical applications. The problem of finding equivalent finite-dimensional models for the Volterra representation (5) has been studied by several authors including *Sontag* [1979] and *Fliess* and *Normand-Cyrot* [1982]. A similar problem involving discrete-time response functions has been investigated by *Leontaritis and Billings* [1987]. They derived a class of finite-dimensional recursive nonlinear input-output models described in terms of a finite number of parameters which can be estimated from data. These models are known as NARMAX (Nonlinear AutoRegressive Moving Average with eXogenous inputs) models. The models take the form of a set of nonlinear difference equations which can be viewed as a generalisation of the linear input-output model in equation (4)

$$y(k) = f(y(k-1), ..., y(k-n_y), u(k-1), ..., u(k-n_u), e(k-1), ..., e(k-n_e)) + e(k) \quad (6)$$

where $f(\cdot)$ is some nonlinear function. Typical choices for $f(\cdot)$ are polynomial, rational or wavelet functions expansions. Practically (6) is of the form of the linear difference equation (4) with the addition of nonlinear higher order terms.

The finite dimensional model in equation (6) is equivalent to the infinite Volterra series description in equation (5) but (6) is much more convenient to estimate and to analyse in practice. Estimating the parameters in a nonlinear model (6) from data is however more difficult than estimating a linear model. The main difficulty stems from the fact that the number of all possible combinations of polynomial terms in the model can be very large. Finding the right combination of terms that is appropriate to the data requires searching through all the candidate terms to find the significant terms. This is known as structure selection. Once the model terms are known the corresponding parameters can be estimated. Finally a number of tests can be performed to check the model validity.

Normally linear models are estimated initially. If the linear models fail the validation tests quadratic, cubic or higher order polynomial terms are included. Often, neither the number of model terms nor the type of terms are known in advance. The method used to estimate the model is known as nonparametric regression. The algorithm used in this paper, *Chen et al* [1989], selects the model terms in an iterative manner until a given error tolerance is achieved and estimates the unknown parameters. Validation tests are then used to validate the identified model using correlation based tests that detect possible unmodelled dynamics in the residuals *Billings and Voon* [1986]. Other tests involve comparing the model predicted output with the available experimental measurements. The *model predicted output* is calculated at each sampling time using the previous model *predicted* outputs and measured inputs as opposed to the *one-step-ahead predicted output* which is calculated using previous output measurements in lieu of previous model

predicted outputs. The model predicted output can expose major flaws in the identified model that the one-step-ahead predicted output cannot detect, such as lack of stability and therefore is a more reliable indicator of the validity of the estimated model.

The experimental data set $\mathcal{D}$ is usually divided into two disjoint subsets $\mathcal{D}_1$ and $\mathcal{D}_2$. The first data set $\mathcal{D}_1$ is used to estimate the model while the second data set $\mathcal{D}_2$ is reserved for testing the model. Since the model estimated from $\mathcal{D}_1$ is assumed to have generated the entire data set $\mathcal{D}$, the model should be able to predict equally well the test data set $\mathcal{D}_2$. The goodness of fit between the model predicted output and the data can be assessed in terms of the Root Mean Square Error $RMSE = \sqrt{\sum_{i=1}^{N} e(t_i)^2/N}$ or by computing the coherency function between the experimental and model generated data.

3 Wave phenomena in the fore-shock

The regions in which ion fluxes are streaming upstream along the magnetic field from the terrestrial bow shock form the ion fore-shock. *Gosling et al., 1978 and Paschmann et al.,* [1979] have shown that these ion populations fall into three distinct classes *reflected, diffuse* and *intermediate* . *Hoppe et al.,* [1981] established that distinct types of turbulence correspond to these types of ion population. They have shown that typical waves associated with the diffuse ion populations are strongly compressional waves which possess a tendency towards steepening into shock like structures. *Hoppe et al.,* [1981] proposed the term shocklets to describe such structures. Often a discrete wave packet can be observed at the upstream edge of shocklets. *Hoppe et al.,* [1981] determined the dispersion of these discrete wave packets from the ISEE data and identified them as whistler waves.

Schwartz et al., [1988], and *Schwartz* [1991] proposed the subdivision of nonlinear wave phenomena observed in the vicinity of the front of a quasi-parallel shock into two types. The first type includes structures "nested" relative to the shock. Nested structures are often regarded as short bow shock encounters. The second type includes structures "convected" with the solar wind. The other classification proposed by these authors subdivided wave structures into relatively short ($\approx$ 10 *seconds*) isolated or identifiable single excursions of the magnetic field (Short Large Amplitude Magnetic Structures, "SLAMS") and longer periods of enhanced, turbulent field, "Long Pulsations" (LPs). Often SLAMS are observed to be embedded in Long Pulsations. *Schwartz et al.,* [1988], and *Schwartz,* [1991] showed that while LPs often show a nested signature all SLAMS observed by them including those embedded in LPs, are convected with the flow. LPs usually have a higher value of *beta*.

Some studies attribute primary significance to the nonlinear wave phenomena observed in the fore-shock. *Omidi and Winske* [1990] suggest that the deceleration of solar wind to sub-sonic speed at cometary shocks is due to the interaction with a number of shocklets. *Schwartz and Burgess* [1991] concluded that the front of a quasi-parallel shock could be considered as a superposition of SLAMS, which gradually decelerate the solar wind and lead to the formation of the downstream state. The importance of identification of nonlinear processes in the fore-shock turbulence is therefore related to the role of nonlinear wave phenomena in the formation of the shock front.

4 Results and Interpretation

The wave phenomena investigated were first encountered by AMPTE UKS and then after propagating through the plasma were measured by AMPTE IRM. Thus the data set measured by AMPTE UKS and by AMPTE IRM were considered to be the input and output of the system, respectively. The same preprocessing procedures used in DW were applied to the data to allow an effective comparison between the two methods (Dudok de Wit private communication).

One thousand pairs of input/output measurements of B_y (the y component of the magnetic field in Figure 1) obtained during the time interval 500-575 seconds past 10:50:00 UT were used in the identification.

A cubic polynomial model was identified from these data. The identified model was simulated using the AMPTE UKS data as the input and the resulting model predicted output was compared with the original AMPTE IRM measurements used to identify the model. Figure 2 shows the measurements of the B_y component by AMPTE UKS as a solid line (input to the system), AMPTE IRM (output the system) as a dotted line and the model predicted output calculated using the identified model as a dashed line.

Figure 3 shows the B_y component measured by AMPTE UKS, AMPTE IRM and the model predicted output calculated using the identified model over a different time interval. This is the test data set that has not been used for model estimation. Both Figures 2 and 3 show very good agreement between the AMPTE UKS measurements and the model predicted output.

Linear and nonlinear correlation based tests were performed on the residuals to validate the model. The correlation functions shown in Figure 4a,b,c,d,e are within the 95% confidence bands, indicating that the model has captured the dynamics in the data.

The visual evaluation of the model predictions does not illustrate how the model performs over a particular frequency range. This can be investigated by computing the coherency function

$$\Gamma(f) = \frac{P^2_{x,y}(f)}{P_x(f)P_y(f)}$$

where $P^2_{x,y}(f)$ is the magnitude of the cross spectral density of the model predicted output B_y^{IRM} and the AMPTE IRM B_y measurements, while $P_x(f)$ and $P_y(f)$ denote the power spectral density of the model predicted output and the AMPTE IRM B_y measurements respectively. The value of the coherency is bounded between 0 and 1. A value of coherency close to 1 means high correlation between the spectral components of the two data sets. A value close to zero means complete independence between two signals at that particular frequency. The magnitude and phase of the coherency function calculated for the real measurements and the output of the model are plotted in Figure 5a,b.

The coherency estimated from a finite set of data is a statistical value, the distribution of which is related to the real value of the coherency between the two signals. In particular, the variance of the phase is determined by the real value of the coherency. The diagrams show that the coherency is very high (> 0.9) up to the frequency 0.6 Hz, which is the frequency range which contains most of the energy of the turbulence. This frequency range contains both nonlinear waves (in particular SLAMS) with frequencies less than $0.1 - 0.2$ Hz, and important ULF waves such as whistler wave trains of shocklets which are usually observed in the frequency range $0.2 \geq f \geq 0.5$ Hz. The value of the phase is distributed around 0 for the same frequency range implying the absence of an artificial delay in the

derived model. The same interval of data was used in DW to model the nonlinear processes in the frequency domain and, although the coherency function calculated to validate the DW model was relatively high for low frequencies corresponding to SLAMS $f < 0.2\ Hz$, it was very low $\Gamma(f) < 0.35$ in the frequency range which corresponds to the whistler wave trains. Such a low coherency implies that the DW model has failed to describe the dynamics of this second class of waves accurately. In contrast, the high coherency of the NARMAX model indicates that this model describes the dynamics of both SLAMS and the whistler packets and possible energy exchange between them very well.

The NARMAX polynomial model can be decomposed into its components to allow the linear, quadratic and cubic contributions to be studied separately

$$\begin{aligned} B_y^{IRM}(k) &= \sum_i a_i B_y^{UKS}(k-i) + \sum_{i,j} b_{i,j} B_y^{UKS}(k-i) B_y^{UKS}(k-j) + \\ &\sum_{i,j,p} c_{i,j,p} B_y^{UKS}(k-i) B_y^{UKS}(k-j) B_y^{UKS}(k-p) \end{aligned} \tag{7}$$

or

$$\hat{B}_y^{IRM} = B_y^{IRM,l} + B_y^{IRM,q} + B_y^{IRM,c} \tag{8}$$

where $B_y^{IRM,l}$, $B_y^{IRM,q}$ and $B_y^{IRM,c}$ represent respectively the linear, quadratic and cubic components of the model.

The linear part of the model can be used to compute the true linear frequency response function $H_1(j\omega)$ the magnitude of which accounts for the change of the wave amplitude due to the interaction with the plasma and the linear wave propagation effect.

The magnitude of $H_1(j\omega)$ calculated from the identified NARMAX model (7) is plotted in Figure 6. In the lower frequency range $f \leq 0.325$, $H_1(j\omega)$ is greater than unity which corresponds to the instability pumping energy into turbulence. This frequency range corresponds to the nonlinear ULF waves and SLAMS which were assumed to grow as a result of the unstable ion distribution. At higher frequencies, which correspond to whistler wave trains and to discrete whistler wave packets, $H_1(j\omega)$ is less than 1 and reflects the damping of the waves and energy transfer from turbulence to the plasma.

The significance of the linear, quadratic and cubic contributions to the dynamics of turbulence can be illustrated using a particular nonlinear wave, SLAMS according to Schwartz, which was observed during the interval 360-400 seconds past 10:50:00 UT. In Figure 7 the original AMPTE IRM (output) measurements B_y^{IRM} (solid) are plotted together with the model predicted output (dashed line), the linear $B_y^{IRM,l}$ (dashed-dotted) and the sum $B_y^{IRM,q} + B_y^{IRM,c}$ (dotted) of the quadratic and cubic components of the model output. From this figure it is evident that the linear part of the model provides a relatively good representation of the evolution of the wave field, close to the model predicted output which provides a very good match to the original data. The nonlinear contribution is non-negligible only in the regions where the magnetic field gradient is significant.

The real measurements of the same SLAMS (dashed), the quadratic (dashed-dotted line) and cubic (solid line) contributions to the model are plotted in Figure 8 together with the difference Δ_{linear} (dotted line) between the measured output and the output of the linear part of the model. It is evident from Figure 8 that the contribution of the cubic term almost coincides with δ_{linear} at the beginning of the whistler wave train whilst the contribution of the quadratic component $B_y^{IRM,q}$ is very small. This indicates that the

effect of the quadratic nonlinearities on the dynamics of the wave field is less important than that of the higher order nonlinearities.

The majority of the other nonlinear waves and discrete wave packets have similar dynamics. Their evolution can be described with good accuracy in terms of the linear part of the model except at the upstream edges of the nonlinear waves. If a whistler wave train is attached to the upstream nonlinear wave, the nonlinear contribution is usually significant at the interface between them. Outside that interface the dynamics of both can be described with good accuracy by linear terms only.

All nonlinear waves except high amplitude whistler packets have such dynamics. The dynamics of the latter is affected by an additional nonlinear effect which is illustrated in Figures 9,10,11. The AMPTE IRM B_y measurements taken during the time interval 600-630 seconds past 10:50:00 UT, plotted as a solid line, are superimposed in Figure 9 with the model predicted output B_y^{IRM} calculated using the identified model (dashed line) and the output $B^{IRM,l}$ corresponding to the linear part of the model (dotted line). Two nonlinear wave phenomena were observed during this time interval. The first of these is SLAMS observed during the time interval 604-610 seconds which is followed by a high amplitude wave packet. While the evolution of SLAMS follows the pattern described above, and can accurately be described by a linear process except around the edge region, the large amplitude wave packet shows different dynamics.

Although the model predicted output calculated using identified NARMAX model follows very closely this large wave packet (dashed line in Figure 9), there is an obvious phase shift between the linear part of the model predicted output (dotted line in Figure 9) and the real measurements (solid line in Figure 9). This indicates that the linear part of the model fails to provide the correct "phase" velocity for this wave packet. The measurements taken by the AMPTE IRM satellite over the same time interval (solid line), the output of the linear part of the model (dotted line) and output of the cubic part of the model (dashed-dotted line) are plotted in Figure 10. This reveals that the contribution due to the cubic nonlinearity is very significant. The actual role of the cubic nonlinearity in correcting the phase of the linear part of the model is obvious in Figure 11, where the real measurements (solid line) are superimposed with the cubic component $B_y^{IRM,c}$ of the model output (dash-dotted) and the linear model error Δ_{linear} (dotted line). In the present paper we will limit our analysis of the evolution of nonlinear waves to these two examples. A more comprehensive analysis of different types of wave events is the subject of a further paper.

5 Discussion and comparison with frequency space identification

Many previous studies of the nonlinear waves in the part of the fore-shock considered in this study pointed to the possible steepening of the upstream edge of the observed waves. Such steepening can be attributed to fundamental nonlinear effects. In particular, the fact that the effect of the nonlinear terms in our model on the wavefield dynamics is important only at the upstream edge of SLAMS, is consistent with the effects of the usual gasodynamic nonlinearity related to the terms $\partial V/\partial t + V\nabla V$ in the isothermal gas motion or in the equations of ordinary hydro- or magneto-hydrodynamics. In such media, initially finite amplitude waves will steepen up.

In frequency space such an effect leads to the coupling of spectral components and the

transfer of energy to higher frequencies and smaller spatial scales. In the frequency space the steepening can be described as a generation of smaller scales in wave-wave interaction processes [*Sagdeev and Galeev,* 1969]. In the case of SLAMS, *Akimoto et al.,* [1991] proposed another scenario in which steepening occurs as a result of plasma instability. That is, the presence of the ions reflected from the shock give rise to resonant electromagnetic ion-ion instability. The fastest growing mode is saturated by trapping the ion beam. According to this model two effects can contribute to the wave steepening. First, the spatially bunched ion beam can generate localised waves. Second, as the beams slow down they will resonate with the waves of shorter wavelength. Both effects will result in the apparent steepening of the original wave.

Our results endorse the usual model of wave steepening because they show that the cubic nonlinearity (i.e four wave coupling) plays a significant role in the steepening of the leading edge of SLAMS and the transfer of energy to the attached whistler wave train.

The second nonlinear effect which has been observed is a contribution of nonlinearity to the propagation velocity of high amplitude nonlinear wave packets. Such an effect also has a straightforward theoretical explanation. In some theoretical studies [*Mjolhus and Wyller* (1986)] it has been shown that quasi-parallel, circularly polarised MHD waves of finite amplitude obey the Derivative Nonlinear Schröedinger (DNLS) equation

$$\frac{\partial b}{\partial t} + \alpha \frac{\partial}{\partial x}\left(|b|^2 b\right) + i\beta \frac{\partial^2 b}{\partial x^2} = 0$$

where α and β are the model parameters. The solution of this equation takes the form:

$$b(x,t) = A_0 \exp\left[i(kx - \omega t)\right]$$

where $\omega = \alpha A_0^2 k - \beta k^2$. Thus the dependence of the phase velocity $V_{ph} = \frac{\omega}{k}$ on the amplitude A_0 is due to the cubic nonlinearity.

Previously *Dudok De Wit et al.,* [1995] pointed out a similar effect as a possible explanation of the differences between maxima in the joint frequency-wave number spectrum and the joint frequency-wave probability density. However the comparison of the joint frequency-wave number spectrum and joint frequency-wave probability density did not provide a definite experimental answer regarding the significance of involvement of a particular type of nonlinearity in that process.

It is worth comparing our results with those obtained by DW for the same interval of data using frequency domain modelling. DW concluded that as the linear processes govern the dynamics of SLAMS the quadratic processes are equally important to the dynamics of whistler wave packets (see Figure 13 in DW). The quadratic contribution is therefore considered significant through the whole whistler wave packet. In contrast our results indicate that the nonlinear effects are confined to the interface between the whistler precursor and SLAMS.

In the DW model the quadratic nonlinearity is essential for the whole whistler wave precursor. DW interprets this nonlinearity as three wave coupling which transfers energy from the SLAMS to the precursor. However such a nonlinear coupling can take place in a particular point of space-time only if both whistler wave precursor and SLAMS coexist at that point which is not possible. Therefore such energy transfer can only take place at their interface point, which is in agreement with our results, and not through the whole whistle precursor, as would happen if the DW model were correct.

The other important issue concerns the role played by three wave interaction processes (quadratic nonlinearity) in the dynamics. Unlike in the DW model, the results of our study

reveal that the influence of the quadratic nonlinearity is very small compared to the effect of higher order nonlinearities. In particular our analysis shows that the contribution of four wave processes (which correspond to the cubic nonlinearity) exceeds the contribution of three wave processes (quadratic nonlinearity).

An important argument to support the validity our model in this context is given by comparing the time-domain identification approach used to derive it with the frequency domain approach employed by DW.

There are two major steps in identification of the mathematical model of a physical input-output system from experimental data. The first is to determine the "structure" of the model i.e. the order of the nonlinearity and the terms involved. The next step involves estimating the parameters associated with this model structure. The algorithm used in this study to estimate our model performs model structure selection and parameter estimation. The algorithm can deal with real noisy measurements and allows the estimation of a noise model which ensures unbiased parameter estimates. As a major advantage, this approach requires relatively small data sets.

There are two major disadvantages of the frequency domain method proposed for the laboratory turbulence by *Ritz and Powers* [1986] and used in DW. The first is that this approach requires that the structure of the mathematical model should be known. In the case of the DW paper for example, this means deciding which of three types of dynamic interactions should be included in the model, linear $\omega \leftrightarrow \omega$, quadratic (i.e. three wave processes of a decay instability type $\omega_1 + \omega_2 \leftrightarrow \omega$), cubic (i.e. four wave processes of a modulational instability type $\omega_1 + \omega_2 + \omega_3 \leftrightarrow \omega$), and which, if any, should be disregarded.

But the main disadvantage of using this approach to analyse space plasma turbulence is the enormous amount of data required to fit parameters to a model that accounts for cubic nonlinearities. This precludes taking into account four wave processes despite the fact that the cross-tricoherence estimated in DW indicate that four-wave interactions have a considerable role in the dynamics of turbulence.

This may explain why the cross-coherency between the real measurements of the magnetic field by AMPTE IRM and the output of the DW model is lower than 0.3 for the frequency range that corresponds to the discrete wave packets. This is a strong indication that the DW model is not an accurate description of the physical processes which take place in plasma in the vicinity of the terrestrial bow-shock.

In contrast to the frequency domain method of Ritz and Powell the time domain analysis based on the NARMAX model does not assume any prior knowledge of the structure of the system. The model structure determination is an inherent part of the identification procedure.

6 Conclusions

This study has demonstrated the potential of the NARMAX approach for the identification of the processes in space plasma turbulence. The main advantages of this method compared with the direct multi-spectrum estimation approaches previously adopted, are the realistic amount of data that is required for the identification and the fact that the resulting NARMAX model appears to provide a far more accurate description of the dynamics with far fewer adjustable parameters than the low-order truncated Volterra expansions used in the frequency domain approach proposed by Ritz and Powers [1986]. Although such fundamental nonlinear processes as wave steepening and nonlinear phase

velocity shifts have been known from analytical studies for a long time, until now there has not been much explicit experimental evidence of their importance in the dynamics of turbulence in space plasma.

7 Aknowledgements

DC and SAB gratefully acknowledge that part of this work was supported by EPSRC.

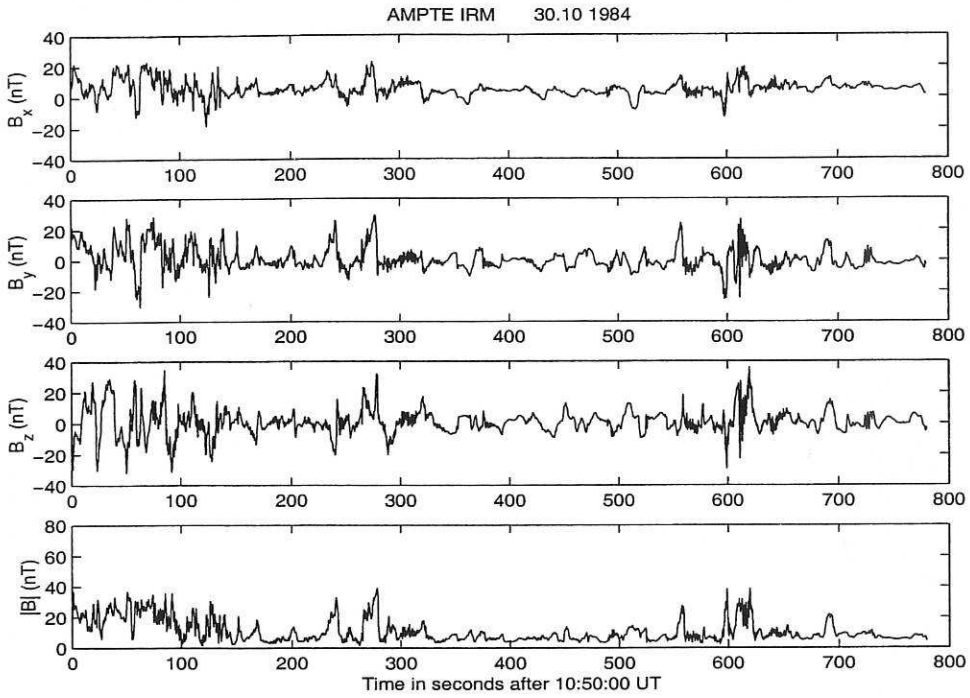

Figure 1: *The magnitude and GSE components of the magnetic field measured by AMPTE IRM during the period on 30th October 1984. Time in seconds after 10:50:00 UT*

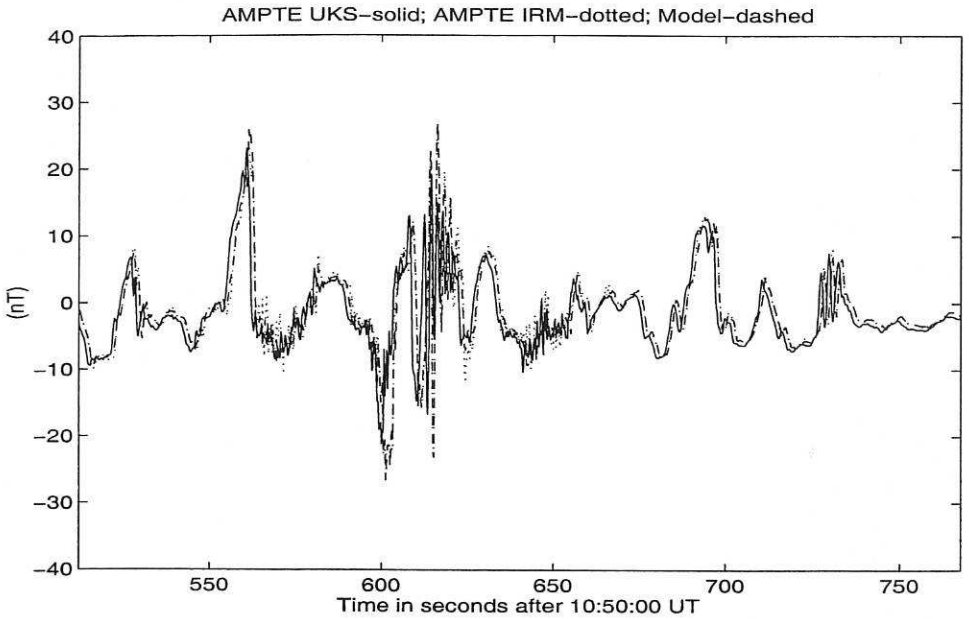

Figure 2: *The B_y GSE components of the magnetic field measured by AMPTE UKS (solid line), AMPTE IRM (dotted line) and the model predicted output of the identified time domain model (dashed line) over the estimation interval. Time in seconds after 10:50:00 UT on 30^{th} October 1984.*

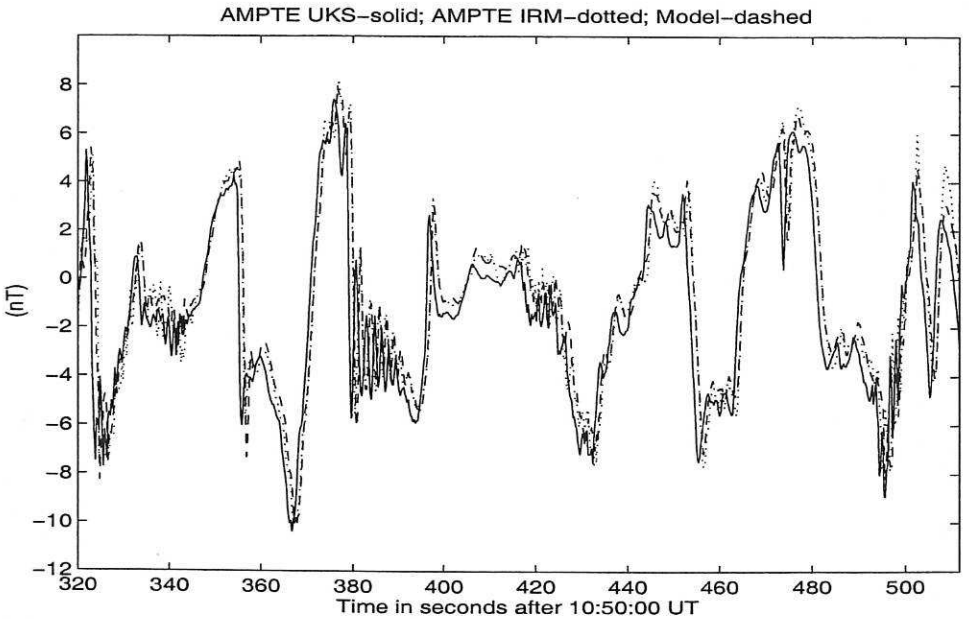

Figure 3: *The B_y GSE components of the magnetic field measured by AMPTE UKS B_y^{UKS} (solid line), AMPTE IRM B_y^{IRM} (dotted line) and the model predicted output of the identified time domain model (dashed line) over the validation interval. Time in seconds after 10:50:00 UT on 30^{th} October 1984.*

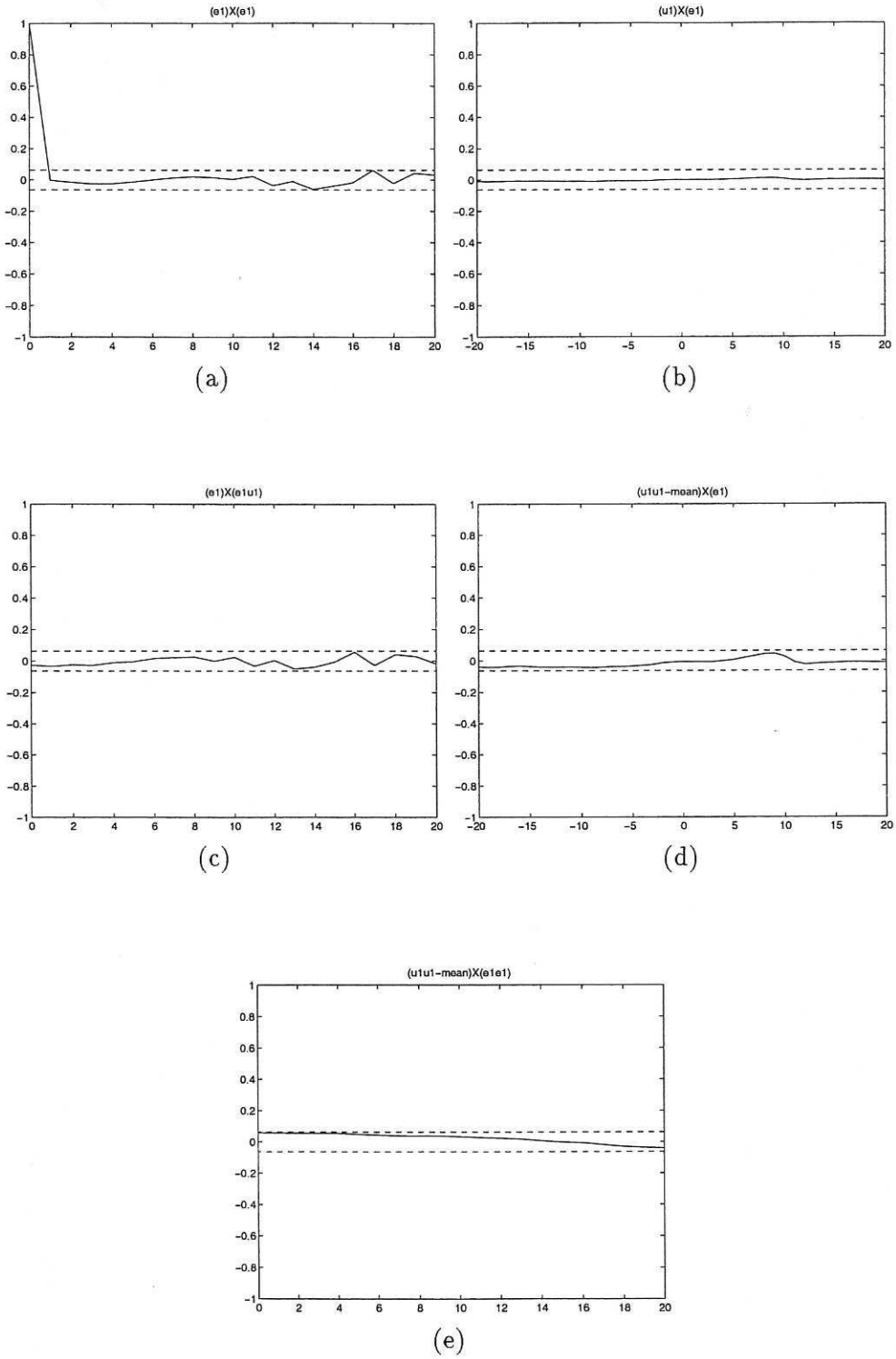

Figure 4: *Correlation based Model Validity Tests - (a)* $\Phi_{\varepsilon,\varepsilon}(\tau)$, *(b)* $\Phi_{u,\varepsilon}(\tau)$, *(c)* $\Phi_{\varepsilon,(\varepsilon u)}(\tau)$ *(d)* $\Phi_{u^2,\varepsilon}(\tau)$, *(e)* $\Phi_{u^2,\varepsilon}(\tau)$. *Dashed line 95% confidence interval*

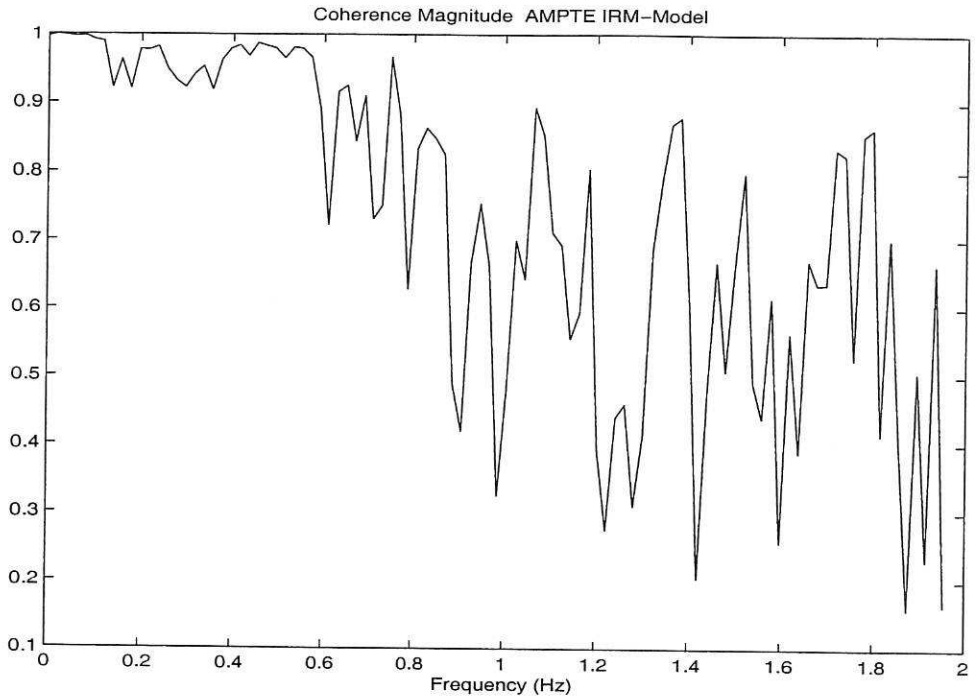

(a)

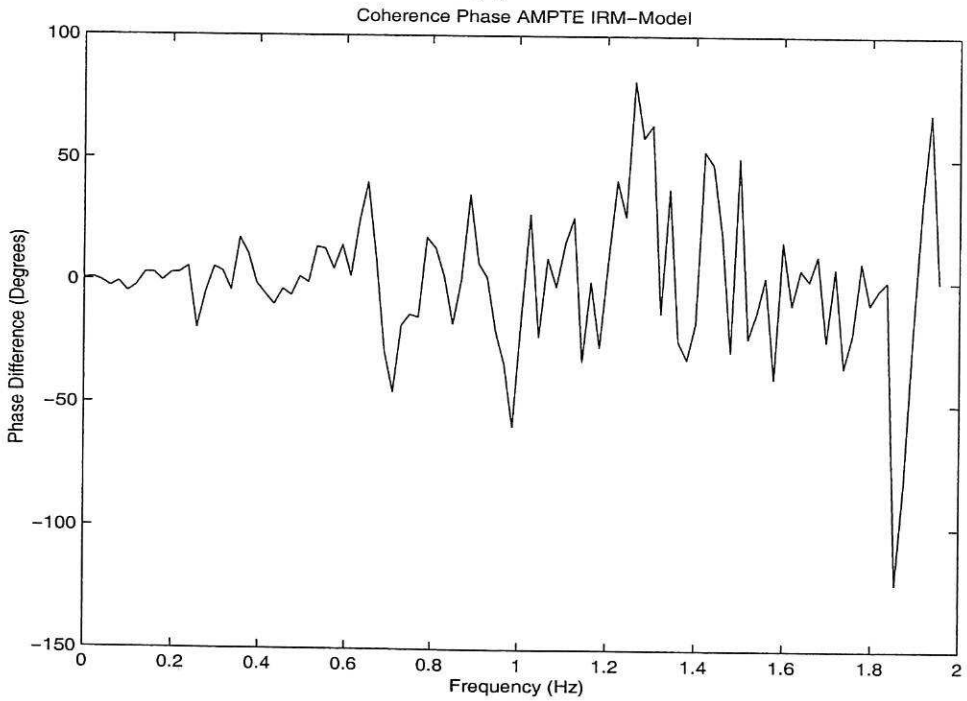

(b)

Figure 5: *(a) The magnitude and (b) the phase of the coherency function calculated for* B_y^{IRM} *GSE components of the magnetic field measured by AMPTE IRM and the model predicted output of the derived time domain model.*

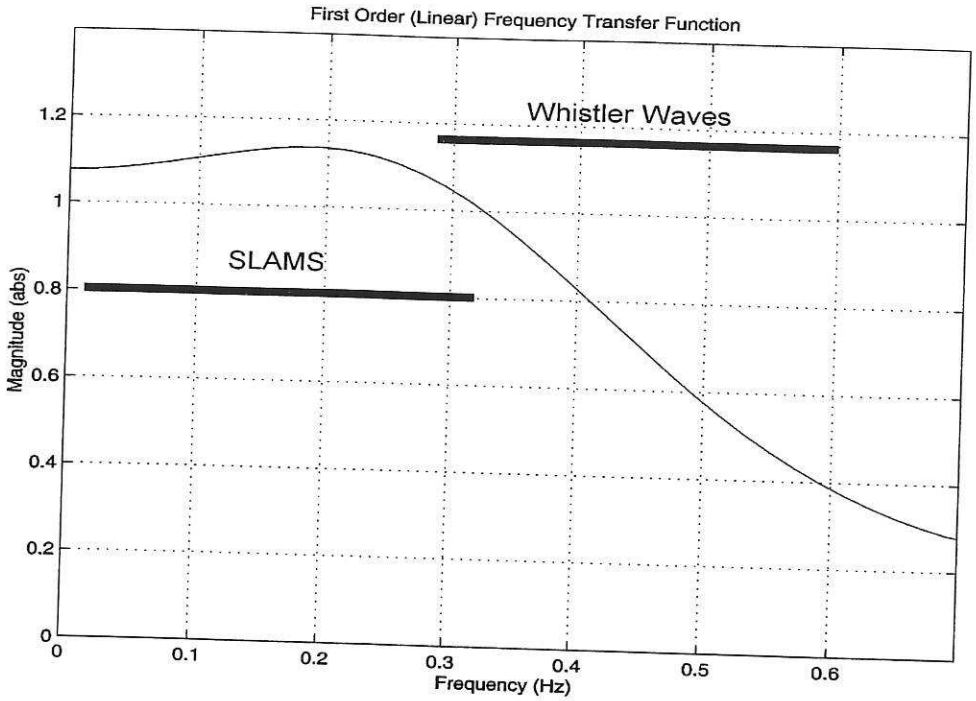

Figure 6: *Magnitude of the first order (linear) transfer function*

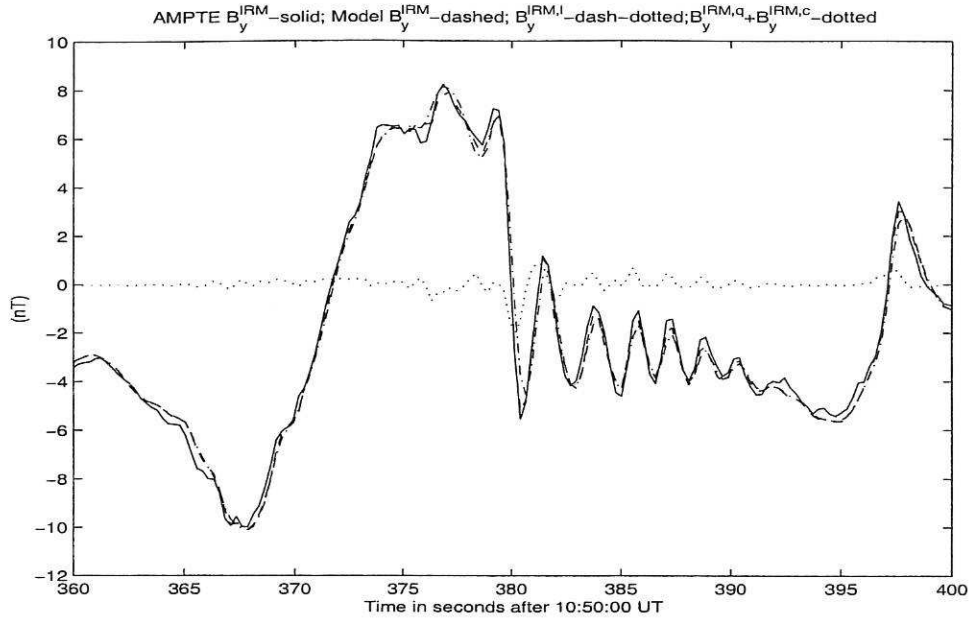

Figure 7: *The B_y GSE components of the magnetic field measured by AMPTE IRM, B_y^{IRM} (solid) are superimposed with the model predicted output (dashed line), the linear $B_y^{IRM,l}$ (dashed-dotted) and the sum $B_y^{IRM,q} + B_y^{IRM,c}$ (dotted) of the quadratic and cubic components of the model predicted output. Time in seconds after 10:50:00 UT on 30^{th} October 1984.*

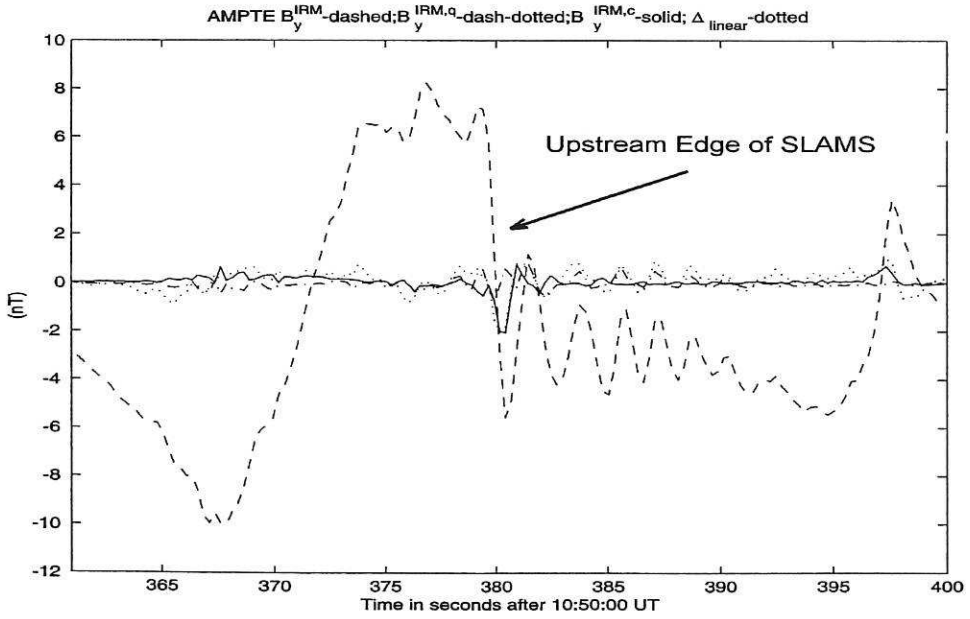

Figure 8: *The B_y GSE components of the magnetic field measured by AMPTE IRM, B_y^{IRM} (dashed) superimposed with the quadratic $B_y^{IRM,q}$ (dashed-dotted line) and cubic $B_y^{IRM,c}$ (solid line) contributions and the difference Δ_{linear} (dotted line) between the real data and the output of the linear part of the model. Time in seconds after 10:50:00 UT on 30^{th} October 1984.*

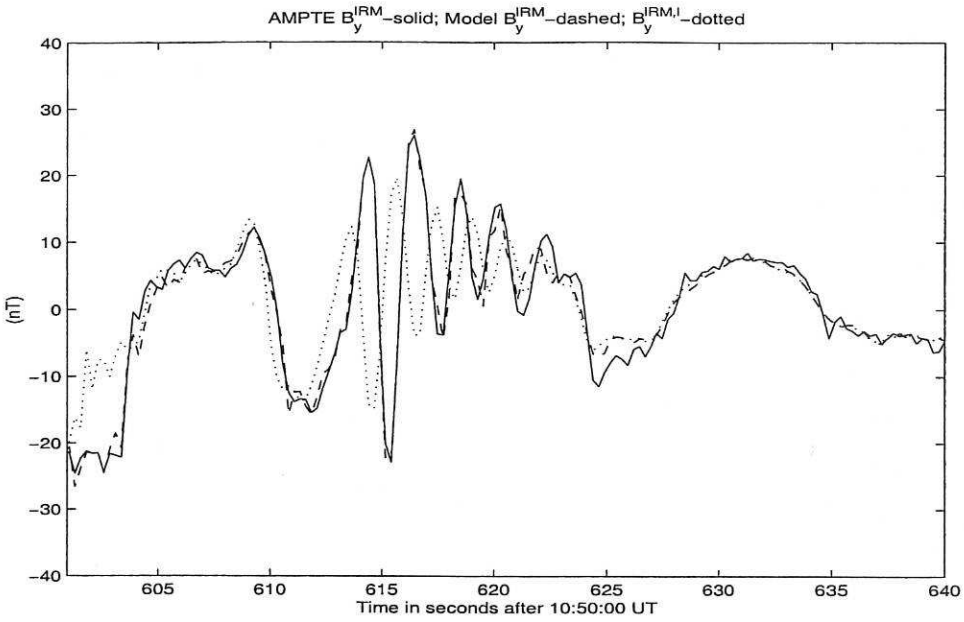

Figure 9: *The B_y GSE components of the magnetic field measured by AMPTE IRM, B_y^{IRM} (solid) superimposed with the output $B^{IRM,l}$ corresponding to the linear part of the model (dotted line) and the output $B_y^{IRM,c}$ of the cubic part of the model (dash-dotted line). Time in seconds after 10:50:00 UT on 30th October 1984.*

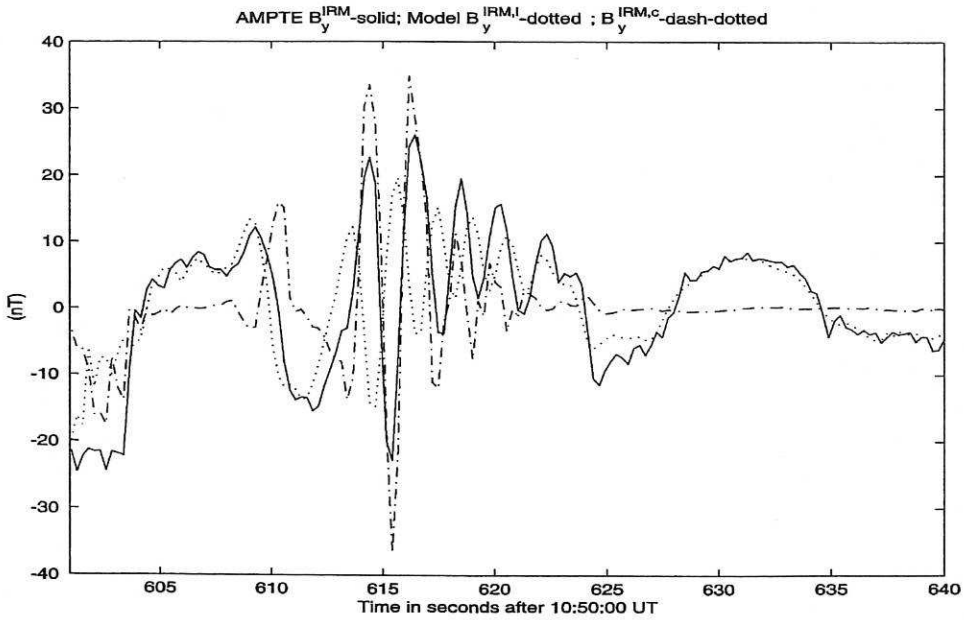

Figure 10: *The B_y GSE components of the magnetic field measured by AMPTE IRM, B_y^{IRM} (solid) superimposed with the model predicted output of the identified model B_y^{IRM} (dashed line) and the output $B^{IRM,l}$ corresponding to the linear part of the model (dotted line). Time in seconds after 10:50:00 UT on 30th October 1984.*

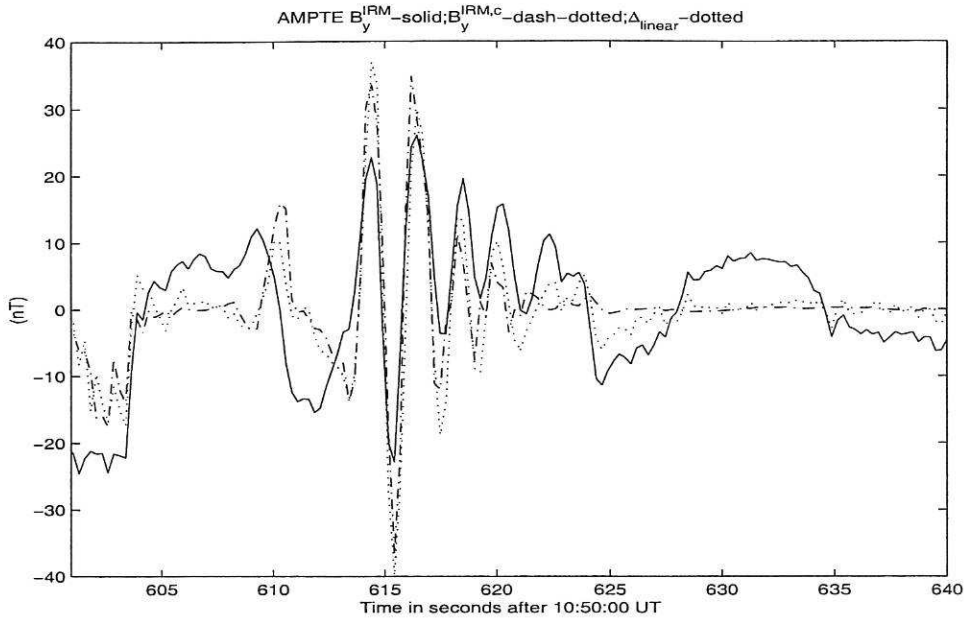

Figure 11: *The B_y GSE components of the magnetic field measured by AMPTE IRM, B_y^{IRM} (solid) superimposed with the output $B^{IRM,c}$ corresponding to the cubic part of the model (dash-dotted line) and with the difference Δ_{linear} between the real data and the output of the linear part of the model (dotted line). Time in seconds after 10:50:00 UT on 30^{th} October 1984.*

References

Akimoto, K., D. Winske, T. G. Onsager, M. F. Thomsen, and S.P. Gary, Steepening of parallel propagating hydro-magnetic waves into magnetic pulsations, *J. Geophys. Res., 96,* 17599, 1991.

Bendat J. S. and A. G. Piersol, Random Data Analysis and Measurements Procedures, John Wiley and Sons, NY, 1986.

Billings, S. A. , W. S. F. Voon, Correlation based model validity tests for non-linear models, *International Journal of Control, 44*, 235, 1986.

Dudok de Wit T., V.V. Krasnosel'skikh, S.D. Bale, M.W., Dunlop, H. Lühr, S.J. Schwartz and L.J.C. Woolliscroft, *Geophys. Res. Lett, 22,* 2653, 1995.

Dudok de Wit, T., V. V. Krasnosel'skikh, M. Dunlop, and H. Lühr, Identifying nonlinear wave interactions in plasmas using two-point measurements, *J. Geophys. Res., 104,* 17079, 1999.

Lühr, H.,N. Klöckler, W. Oelschägel, B. Häusler, and M. Acuna, The IRM magnetometer, *The IEEE Trans. Geosci. and Remote Sensing GE-23,* 259, 1985.

Hope, M. M., C. T. Russell, L. A. Frank, T. E. Eastman, and E. W. Greenstadt, Upstream hydromagnetic waves and their association with backstreaming ion populations: ISEE-1 and 2 observations, *J. Geophys. Res., 84,* 4471, 1981.

Fliess, M. , D., Normand-Cyrot, On the approximation of nonlinear systems by some simple state-space models, *Proc. IFAC Symp. on Identification and System Parameter Estimation*, 1982.

Leontaritis, I. J., S. A. Billings, Input-output parametric models for nonlinear systems-Part 1: Deterministic non-linear systems:Part 2:Stochastic non-linear systems, *International Journal of Control, 41*, 303, 1987.

Mann G., H. Lühr, W. Baumjohann, Statistical stuy of short large amplitude magnetic field structures in the vicinity of the quasi-parallel bow shock, *J. Geophys. Res., 99* 13315, 1994.

McCafrey, D. , I. Bates, M. A. Balikhin, H.St. C. K. Alleyne, M. Dunlop, W. Baumjohann, Experimental method for identification of dispersive three wave coupling in space plasma, *Adv. Space Res, 25,* 1571, 2000.

Ritz Ch.P., E. J. Powers, Estimation of nonlinear transfer functions for fully developed turbulence, *Physica, 20D*, 320, 1986.

Schwartz, S. J., R. L. Kessel, C.C. Brinca, L.J.C. Woolliscroft, M. Dunlop , C.J. Farrugia and D.S. Hall, Active current sheets near the Earth's bow shock, *J. Geophys. Res., 93,* 11295, 1988.

Schwartz, S. J., and D. Burgess, Quasi-parallel shocks: a patch-work of three-dimensionless structures, *Geophys. Res. Lett, 18,* 373, 1991.

Schwartz, S. J., D. Burgess, W. P. wilkinson, R. L. Kessel, M. Dunlop , and H. Lühr, Observation of short large amplitude magnetic field structures at a quasi-parallel shock, *J. Geophys. Res., 97,* 4209, 1992.

Sontag, E. D., Polynomial response Maps, Lecture Notes in Control and Information Sciences 13, Berlin:Springer Verlag, 1976.

Southwood, D.J., W.A.C. Mier-Jedrzejowicz, and C.T. Russell, The fluxgate magnetometer for the AMPTE UKS subsatellite, *IEEE Trans. Geosci. and Remote Sensing GE-23*, 301, 1985.